



Cite this: RSC Adv., 2015, 5, 47766

Photodegradation and antibacterial studies of ZnS enwrapped fly ash nanocomposite for multipurpose industrial applications

Kalyanaraman Kalpana and Vaithilingam Selvaraj*

A ZnS-enwrapped amine-functionalized fly ash nanocomposite (ZnS/A-FA) has been prepared by using various weight percentages of amine functionalized fly ash, zinc nitrate hexahydrate and sodium sulphide through wet chemical synthesis method. The synthesized ZnS/A-FA photocatalyst is characterized using XRD, UV-visible DRS, PL, FT-IR, FE-SEM, EDX, elemental mapping, HR-TEM, TGA and BET techniques. The BET surface area results conclude that the fly ash-supported ZnS has a higher surface area of $153.5\text{ m}^2\text{ g}^{-1}$ than that of bare ZnS ($68.5\text{ m}^2\text{ g}^{-1}$). The photocatalytic activity of the ZnS/A-FA nanocomposite has been investigated for the degradation of methylene blue (MB) dye under UV irradiation. The percentage dye degradation experiments are conducted by varying the weight percentage of A-FA supported ZnS to 0.25%, 0.5%, 1%, 2% and 3%. In addition, kinetic studies are carried out by varying the pH, catalyst dosage of ZnS-enwrapped A-FA nanocomposite and dye concentration. From the results, it has been concluded that the fly ash-supported ZnS shows higher catalytic activity compared to that of bare ZnS nanoparticles. Further, one weight percent A-FA-supported ZnS nanocomposite exhibits higher photocatalytic performance when compared to other ratios. The antibacterial properties of A-FA, bare ZnS and the ZnS/A-FA nanocomposite are studied against Gram-positive and Gram-negative bacteria. From the antibacterial studies, it has been found that the ZnS-enwrapped A-FA material exhibits good antibacterial activity compared to that of A-FA and bare ZnS nanoparticles. Hence, ZnS-enwrapped fly ash is a promising photocatalyst for waste water treatment, dye degradation and antibacterial applications.

Received 18th December 2014
Accepted 29th April 2015

DOI: 10.1039/c4ra16642f
www.rsc.org/advances

Introduction

Thermal power plants generate fly ash (FA) as a byproduct, which is dumped day by day as tons and tons of FA material. It causes pollution to the air, water and land. Further, it appears as land fill that can pollute surface and ground water, becoming a major form of environmental pollutant. By considering the overall concern for the environment, there is a need for the safe disposal and efficient utilization of FA material. To minimize the environmental issues (air, water and land pollution), a useful and economical route for the effective exploitation of FA can be employed. FA is rich in aluminosilicate and it possesses unique, stable, abundant, economical and low density particles.¹ Hence, this paves the way to use FA as a supporting material for semiconductor nanoparticles towards heterogeneous photocatalysis. Heterogeneous photocatalysis has shown to be a potent technique for solving various environmental crises.^{2,3} Titanium dioxide (TiO_2) is highly stable, nontoxic,

cheap^{4–6} and has been proven to be an efficient photocatalyst for the degradation of organic pollutants.^{7,8} Among other semiconductor materials, ZnS is one of the most important semiconductors and it has been used as a potent catalyst for the photodegradation of organic dyes.^{9,10} ZnS is a direct wide band gap semiconductor (3.72 eV) and its photocarrier generation ability has found to be higher than that of TiO_2 , which improves the efficiency of the catalyst. Hence, ZnS shows enhanced photocatalytic activities compared to TiO_2 .¹¹ ZnS has wide variety of applications in the fields of LEDs, electroluminescence, flat panel displays, infrared windows, lasers, biodevices, optical coatings, electro-optic modulators, photoconductors, optical sensors, phosphors, etc.¹² In the case of semiconductor nanoparticles, photocatalytic reactions are suppressed mainly due to aggregation of the nanomaterials, lower adsorption capacity, decreased surface area and reduced recyclability of the catalyst. In order to overcome such drawbacks, porous materials like silica, alumina, activated carbon and Mobil Crystalline Material (MCM) are used as supports for metal sulfide or metal oxide photocatalysts. The specific surface area and adsorption efficiency of the catalyst has found to be improved in the presence of a supporting material. Further, the presence of semiconductors on the supporting material inhibits the

Nanotech Research Lab, Department of Chemistry, University College of Engineering Villupuram (A Constituent College of Anna University, Chennai, Kakuppam, Villupuram, 605 103, Tamil nadu, India. E-mail: rajselva_77@yahoo.co.in; vselva@oucev.edu.in; Fax: +91-04146-224500

recombination of electron–hole pairs.¹³ Fly ash is cost effective and it shows good adsorption properties for catalytic applications. Hence, fly ash has been chosen as a supporting material for photocatalytic experiments.^{14–30}

To the best of our knowledge, this is the first report of the synthesis of a ZnS/A-FA nanocomposite for photocatalytic dye degradation and antimicrobial applications. The prime aim of the present investigation is to prepare a ZnS/A-FA nanocomposite for the optimization of A-FA content in the photocatalyst for dye degradation applications. Further, the present article reports the photodegradation of MB dye as a model pollutant under UV illumination. From the results, it has been found that a one weight percent A-FA supported ZnS nanocomposite is an effective catalyst compared to other weight percentages of A-FA-supported ZnS. Further, the antibacterial properties of A-FA, bare ZnS and the ZnS/A-FA nanocomposite are investigated against Gram-positive and Gram-negative bacteria. ZnS-enwrapped fly ash shows higher photocatalytic and antibacterial activities compared to those of the bare ZnS nanocatalyst. Hence, it has been concluded that the ZnS-enwrapped A-FA photocatalyst is a potent photocatalyst towards dye degradation with good antimicrobial properties for waste water treatment applications. The kinetic studies of the photodegradation measurements are carried out by varying dye concentration, catalyst dosage and pH values.

Experimental details

Materials

Fly ash (FA) samples are obtained from a thermal power station in Neyveli, India. Aminopropyltrimethoxysilane (APTMS) is purchased from Sigma Aldrich. Zinc nitrate hexahydrate, sodium sulphide, toluene and absolute ethanol are purchased from Merck. All the chemicals are analytical grade and are used without further purification.

Preparation of A-FA

1 g of FA sample is initially acid functionalized by using 50 mL of 1 M hydrochloric acid and the resultant mixture is stirred at 80 °C for 3 h. The acid-treated FA is washed repeatedly with water until the solution becomes neutral and is dried at 100 °C for further use. 1.0 g of acid-treated FA is dispersed in 10 mL of toluene containing 2 mL of aminopropyltrimethoxysilane. Then, the above mixture is refluxed for 10 h under nitrogen atmosphere. The resulting amine-functionalized fly ash particles are filtered and washed with ethanol. Finally, the product A-FA particles are dried under vacuum at 60 °C for 24 h.¹⁸

Preparation of the ZnS/A-FA nanocomposite

ZnS with various weight percentages of A-FA nanocomposite are prepared by using zinc nitrate hexahydrate ($\text{Zn}(\text{NO}_3)_2 \cdot 6\text{H}_2\text{O}$), sodium sulphide (Na_2S) and various weight percentages of A-FA as precursor materials. Typically, for the synthesis of ZnS with one weight percent of A-FA, 1 wt% of A-FA is dispersed in 100 mL of deionized water. Subsequently, 0.4 M $\text{Zn}(\text{NO}_3)_2 \cdot 6\text{H}_2\text{O}$ is added to the above mixture and stirred for 1 hour. To this, about

100 mL of 0.4 M sodium sulphide solution is added in a drop-wise manner with stirring. The resulting suspension is continuously stirred for a further 2 hours. Then, the final product is centrifuged, washed with distilled water and dried at 80 °C for 5 hours to obtain the ZnS/A-FA nanocomposite. Finally, the synthesized ZnS/A-FA nanocomposite is stored as a fine powder and labeled as 1 wt% ZnS/A-FA nanocomposite. Other weight percentages of ZnS/A-FA material are synthesized under similar experimental conditions using 0.25, 0.5, 2 and 3 weight percent of A-FA. In addition, for comparative studies, bare ZnS is also synthesized under similar experimental conditions in the absence of the A-FA material.

Characterization techniques

Powder X-ray diffraction (XRD) studies are carried out using an XRD-600 model, Shimadzu, Japan. High resolution transmission electron microscopy (HR-TEM) analysis has been conducted with a JOEL JEM-2010 using a 200 kV accelerating voltage. The diffuse reflectance spectra (DRS) are obtained using a Shimadzu UV 2450 model. The photoluminescence spectra are analyzed using a Jasco spectrofluorometer Model FP-8300. The morphology of the sample was determined using field emission scanning electron microscopy (FESEM) and EDX analysis using a Carl Zeiss SUPRA 55 Model. The specific surface area has been determined from nitrogen adsorption at 77 K on the basis of the Brunauer–Emmett–Teller (BET) equation using a Micromeritics ASAP 2020 V3.00 H instrument. The UV-visible spectral measurements are carried out using a Jasco V-650 spectrophotometer.

Photodegradation experiments

The photocatalytic irradiation experiments are carried out using a Heber Scientific multilamp photoreactor. It consists of 8 W medium pressure mercury vapour lamps set in parallel and emitting 365 nm wavelength. The photoreactor has a reaction chamber with a specially designed reflector made of highly polished aluminium and with an inbuilt cooling fan. It is provided with a magnetic stirrer and glass reaction tubes of 50 mL capacity. An aqueous solution of the dye with the catalyst is continuously aerated using a pump for complete mixing of the reaction mixture. For each run, the appropriate amount of catalyst is dispersed in 50 mL of 12 ppm MB dye solution. Prior to illumination, the suspension has been stirred in the dark for 30 min to achieve the adsorption–desorption equilibrium between the catalyst and dye solution. At different UV irradiation time intervals, 2 mL of sample is withdrawn and then centrifuged to remove the catalyst. The supernatant is analysed using a double beam UV-visible spectrometer to measure the concentration of MB dye. Control experiments are also carried out without the photocatalyst under similar experimental conditions.

Antibacterial studies

The antibacterial properties of A-FA, bare ZnS and the ZnS/A-FA nanocomposite have been investigated against *Staphylococcus aureus* (Gram-positive) and *Escherichia coli* (Gram-negative)

bacteria. The test strains are subcultured and incubated for 1 h at 35 °C. After the incubation period, the bacterial culture is swabbed on previously prepared and solidified Muller Hinton agar plates. A disc has been placed on the Petri dish and each disc is inoculated with different concentrations of A-FA, ZnS and the ZnS/A-FA nanocomposite. The bacterial resistances of the A-FA, ZnS and the ZnS/A-FA nanocomposite samples are investigated from the zone of inhibition of the disc. The anti-microbial studies are repeated three times and their respective average results are reported. Thus, the total diameter of the inhibition zone has been evaluated to study the microbial activity.

Results and discussion

XRD analysis

The XRD patterns of amine-functionalized fly ash (A-FA), the ZnS/A-FA semiconductor and bare ZnS nanoparticles are shown in Fig. 1. The XRD spectrum of amine-functionalized fly ash (Fig. 1) indicates that the material is made up of amorphous aluminosilicate glass and crystalline phases of mullite and quartz. Broad XRD peaks are observed for the ZnS/A-FA nanocomposite, which indicates the formation of ZnS nanoparticles in the A-FA material. Diffraction peaks (Fig. 1) are observed in the region of 28.54, 47.45 and 56.34 at 2θ values that correspond to (1 1 1), (2 2 0) and (3 1 1) planes, which can be indexed to ZnS with a cubic structure (JCPDS no. 05 0566).^{31,32} On comparing the XRD spectrum of the A-FA material with the ZnS/A-FA nanocomposite, three new broadened diffraction peaks have appeared for the ZnS/A-FA nanocomposite that are similar to the ZnS nanoparticles, which reveals the formation of the ZnS/A-FA nanocomposite through acid activation and reaction with amine-functionalized fly ash. Further, the intensity of the ZnS/A-FA nanocomposite has decreased compared with the bare ZnS material, which confirms the deposition of ZnS particles on the surface of the A-FA material.

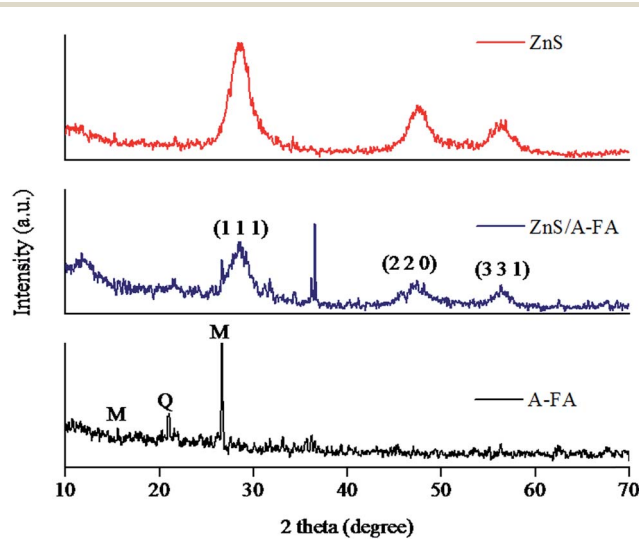


Fig. 1 XRD patterns of amine functionalized fly ash A-FA (M – mullite and Q – quartz), ZnS/A-FA nanocomposite and ZnS nanoparticles.

FT-IR studies

Fig. 2 and 3 show the FT-IR spectra of amine-functionalized fly ash (A-FA) and the ZnS/A-FA nanocomposite.

In the FT-IR analysis (Fig. 2), the appearance of a peak at 2947 cm⁻¹ is due to the C-H stretching vibration. The peaks appearing at 1093 and 1629 cm⁻¹ correspond to C-N stretching and N-H bending vibrations, respectively. In addition, the peak observed at 797 cm⁻¹ represents the N-H wagging vibration of A-FA. The deeper interpretation of the FT-IR confirms that the peak appearing at 3464 cm⁻¹ probably belongs to -NH₂, which is in good agreement with a previous report.¹⁸

In the case of the ZnS/A-FA nanocomposite (Fig. 3), there is no change in the absorption frequencies of any groups except the -NH₂ group, which is now broadened. From these observations, it is clear that the free amino group is responsible for the binding of the ZnS nanoparticles on the surface of the fly ash material. Further, the appearance of peaks at 481, 618 and 1116 cm⁻¹ in the FT-IR spectrum of the ZnS/A-FA nanocomposite are assigned to Zn-S stretching vibrations, which are in agreement with the literature values.^{31,33} Thus, the FT-IR studies confirm the deposition of ZnS on the surface of the A-FA material.

TGA analysis

TGA thermograms are obtained to study the stability of ZnS and ZnS/A-FA by heat treatment from room temperature to 900 °C. The thermograms of ZnS and ZnS/A-FA are shown in Fig. 4. From the TGA data, the weight loss of the ZnS/A-FA nanocomposite has been found to occur at 301 °C, probably due to decomposition of the organic groups present in the nanocomposite. In addition, above 700 °C the nanocomposite exhibits a smooth downward curve, which implies the release of residual sulphur from the ZnS/A-FA nanocomposite. The bare ZnS nanoparticles show an initial weight loss at 159 °C due to the absorption of moisture. Further, the appearance of a smooth curve beyond 700 °C reveals the evolution of sulfur ions

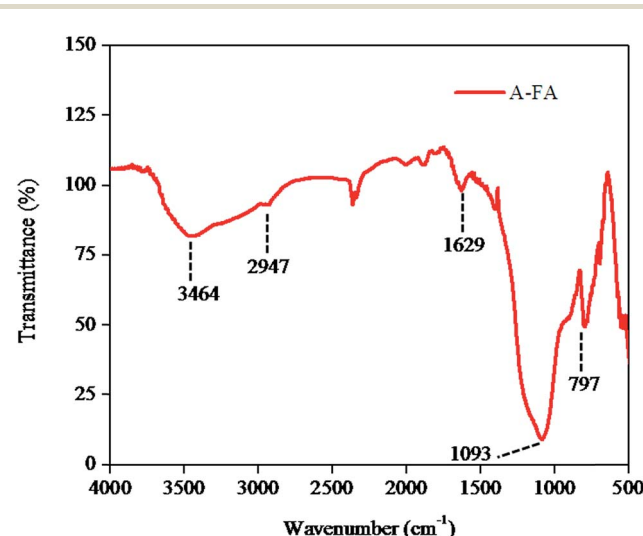


Fig. 2 FT-IR spectrum of amine functionalized fly ash (A-FA).

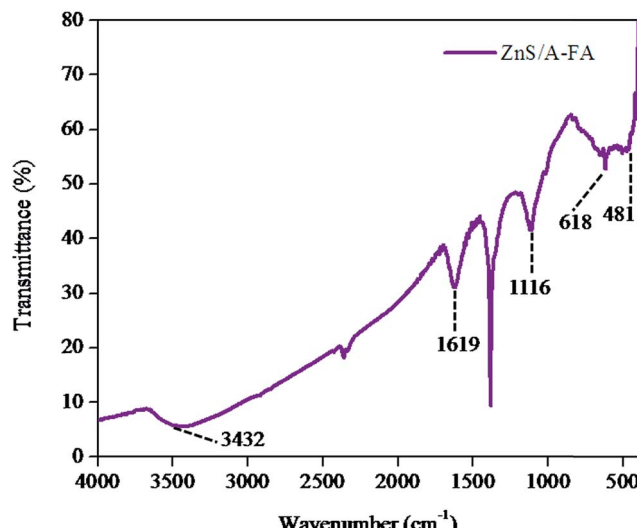


Fig. 3 FT-IR spectrum of ZnS/A-FA nanocomposite.

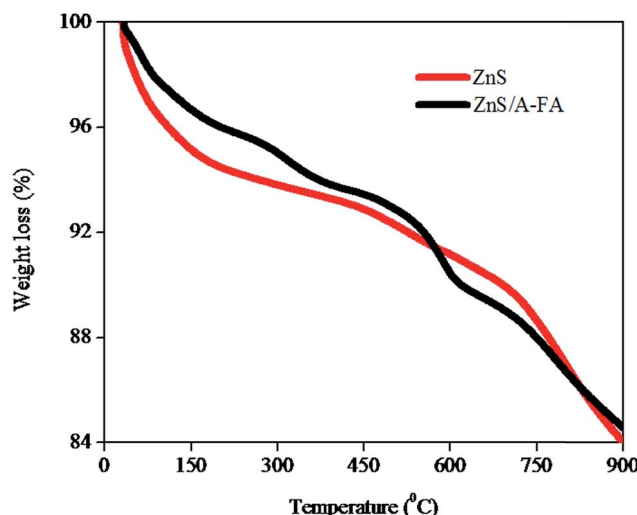


Fig. 4 TGA analysis of ZnS and ZnS/A-FA nanocomposite.

in the ZnS catalyst, as in the case of the ZnS/A-FA nanocomposite. Thus, the above report proves the existence of inorganic metal as a semiconductor in the bare ZnS nanoparticles and the ZnS/A-FA nanocomposite.

UV DRS analysis

The UV diffuse reflectance spectra of bare ZnS and ZnS/A-FA nanocomposite samples are shown in Fig. 5. The UV-visible diffuse reflectance spectra of ZnS and ZnS/A-FA are recorded to investigate the optical properties of the samples. The band-gap energy has been calculated by using following formula according to previous reports:^{34,35}

$$E_{bg} = 1240/\lambda \text{ (eV)} \quad (1)$$

where λ is the wavelength in nanometers and E_{bg} is the photon energy.

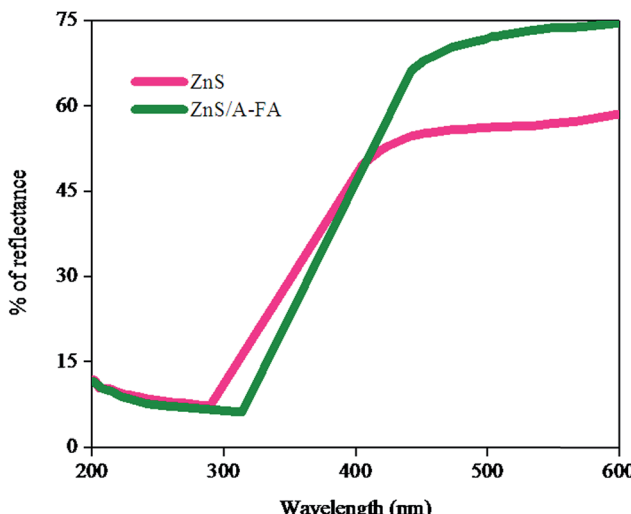


Fig. 5 UV visible DRS spectra of bare ZnS and ZnS/A-FA nanocomposite.

The reflectance spectrum of the ZnS/A-FA nanocomposite shows a red shift when compared with bare ZnS. The calculated band gap energy values of ZnS and ZnS/A-FA are 3.43 and 3.28 eV, respectively. The decrease in the band gap energy of ZnS/A-FA is due to the impact of the A-FA material on the ZnS nanoparticles.^{19,29} Further, this may be due to the synergistic chemical interaction between the A-FA and ZnS nanoparticles present in the ZnS/A-FA nanocatalyst. The decreased band gap energy of the ZnS/A-FA nanocomposite exhibits a broader optical absorption in the UV region than the bare ZnS, so it can be excited to generate more electron–hole pairs under UV irradiation. Thus, the decrease in the band gap energy value of the ZnS/A-FA nanocomposite obviously improves the photocatalytic activity of the catalyst.^{19,29} Hence, the UV DRS studies also provide supporting evidence for the enhancement of the photocatalytic activity of dye degradation for waste water treatment.

Photoluminescence studies

Photoluminescence (PL) studies offer an excellent method for confirming the binding of any fluorescent material to a non-fluorescent material. It is well known that a non-fluorescent material efficiently quenches the emission of photoluminescent materials. PL spectra measurements are recorded for ZnS and various compositions of the ZnS/A-FA nanocomposite at room temperature. Fig. 6 depicts the PL spectra of ZnS and various weight percentages of the ZnS/A-FA nanocomposite. The band edge emission of the bare ZnS nanoparticles and various wt% of ZnS/A-FA appeared at 410 and 450 nm. The low emission peak at 410 nm is ascribed to the surface defects and vacancies of the nanoparticles.^{36–40} From the results, it has been observed that the intensity of the photoluminescence decreases with increasing fly ash content in the ZnS/A-FA catalyst. Hence, the decrease in peak intensity reveals that PL quenching occurs due to the chemical interaction between the ZnS and A-FA material.

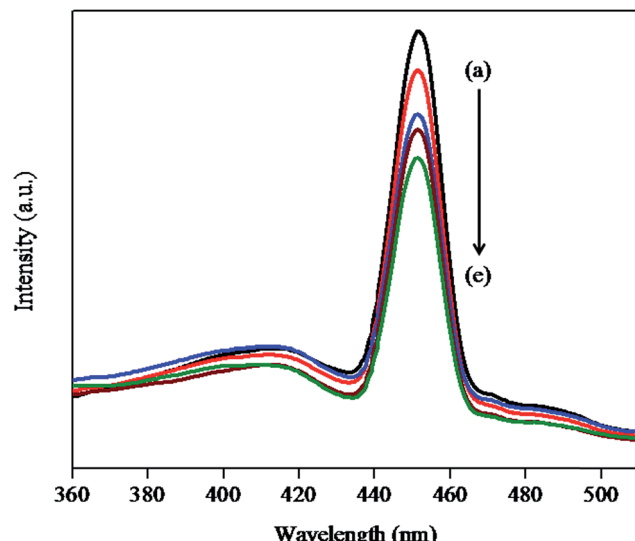


Fig. 6 Photoluminescence spectra of (a) ZnS, (b) 0.25 wt% ZnS/A-FA, (c) 0.5 wt% ZnS/A-FA, (d) 1 wt% ZnS/A-FA and (e) 2 wt% ZnS/A-FA nanocomposite.

Further, the addition of A-FA material to ZnS suppresses the recombination of electron–hole pairs and hence it can be used as an effective catalyst for dye degradation applications.

FE-SEM and EDX analysis

Fig. 7 shows the FE-SEM image, EDX pattern and elemental mapping of the ZnS/A-FA catalyst. The EDX and its mapping display the major constituents present in the ZnS/A-FA composite. The peaks corresponding to Zn, S, Si, C, O and Al that appear in the EDX analysis indicates the existence of fly-ash as the supporting material in the ZnS/A-FA nanocatalyst.⁴¹

Furthermore, the EDX analysis supports the presence of elements such as Zn and S in the ZnS/A-FA nanocomposite. From the FE-SEM and elemental mapping pictures, it is clear that the ZnS nanoparticles are found to be highly dense and homogenously distributed on the surface of the A-FA material. From the above results, it has been concluded that ZnS particles are uniformly distributed on the surface of the A-FA material.

HR-TEM analysis

Fig. 8 shows the HR-TEM images and the corresponding histogram of the ZnS nanoparticles deposited in one weight percent A-FA material. The HR-TEM images exhibit uniform dispersion of ZnS particles over the A-FA material. From the HR-TEM image, it has been possible to visualize the enwrapping of the surface of the A-FA composite by ZnS particles. Further, the histogram clearly shows the size distribution of the ZnS nanoparticles on the surface of the A-FA material. From the results, it has been found that the average size of the ZnS/A-FA nanocomposite is 2–8 nm.

BET analysis

The surface areas of A-FA, ZnS and various weight percentages of ZnS/A-FA are investigated from their nitrogen adsorption–desorption isotherms (Fig. 9). ZnS displays the type II isotherm of non-porous materials, but in the case of the adsorption–desorption curves of the ZnS/A-FA nanocomposite, sharply declining curves are observed for the desorption process, and the nanocomposite exhibits a type IV isotherm curve through capillary condensation with an H4 hysteresis-loop, which shows its predominantly mesoporous nature.^{42,43} The surface area of the catalyst plays a key role in determining the activity of the photocatalyst. Heterogeneous photocatalysis is well known for having surface based processes and a catalyst with a high specific surface area is essential to produce more active sites⁴⁴.

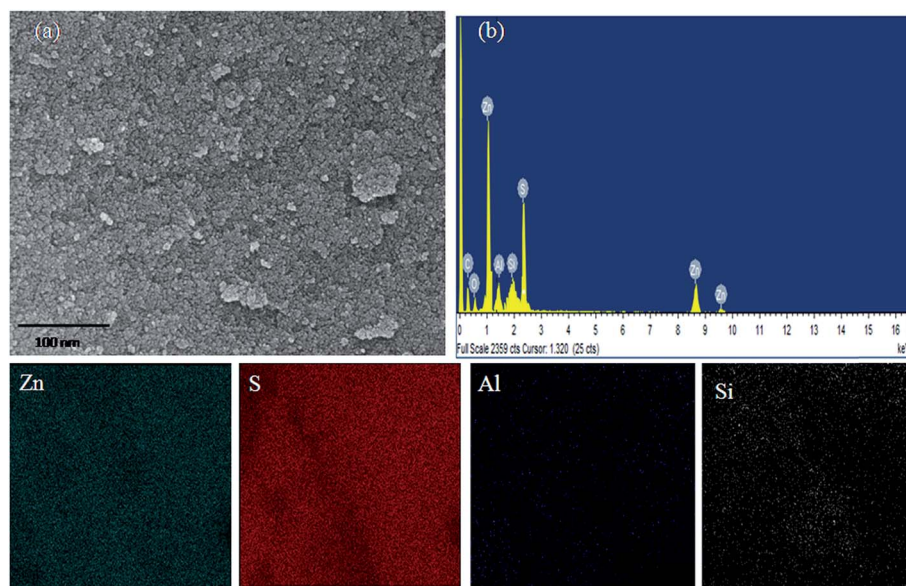


Fig. 7 FE-SEM image (a), EDX spectrum (b) and elemental mapping of ZnS/A-FA nanocomposite.

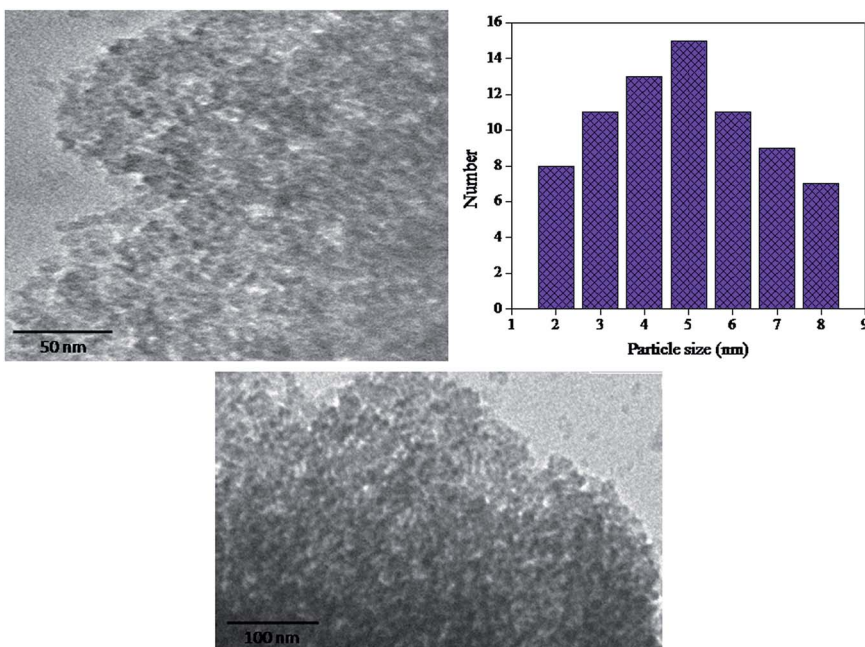


Fig. 8 The TEM images and particle size distribution histogram of ZnS/A-FA nanocomposite.

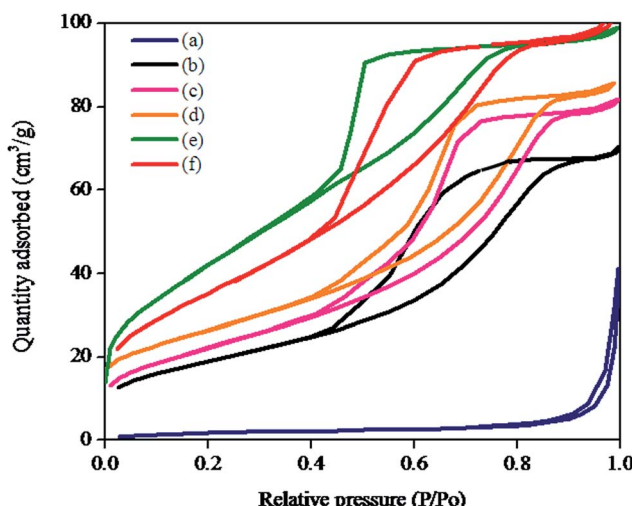


Fig. 9 Nitrogen adsorption–desorption isotherm of (a) A-FA, (b) ZnS, (c) 0.25 wt% ZnS/A-FA, (d) 0.5 wt% ZnS/A-FA, (e) 1 wt% ZnS/A-FA and (f) 2 wt% ZnS/A-FA.

that can increase light reaching the surface of the ZnS/A-FA catalyst, and hence photocatalytic activity could be improved. It has been widely accepted that a porous framework can aid the transportation of reactants and products through the interior spaces owing to the interconnected porous network and this supports the harvesting of excited light due to the enlarged surface area and multiple scattering occurring within the porous structure.⁴⁵ The BET surface areas of A-FA, ZnS, 0.25 wt% ZnS/A-FA, 0.5 wt% ZnS/A-FA, 1 wt% ZnS/A-FA and 2 wt% ZnS/A-FA are 6.7, 68.5, 79.2, 96.3, 153.5 and 130.6 m² g⁻¹, respectively. Thus, 1 wt% ZnS/A-FA possesses a larger surface area than the other weight ratios of A-FA with ZnS material. In addition, the

surface area gradually increased with increasing FA material up to 1 wt%. In the present case, either below or above 1 wt% A-FA content in the composite the specific surface area of the ZnS/A-FA catalyst is reduced. Hence, the 1 wt% ZnS/A-FA nanocomposite has a high surface area, which can increase the number of active adsorption sites. So, the above studies conclude that the photocatalytic activity of the catalyst depends upon the surface area of the material.

Photodegradation of methylene blue (MB)

The photodegradation of MB dye has been carried out in the presence of bare ZnS nanoparticles, A-FA material and various weight percentages of ZnS/A-FA nanocomposite. One weight percent ZnS/A-FA (1 wt%) shows a higher photocatalytic activity compared with the other weight ratios of ZnS/A-FA nanocomposite. Hence, the photodegradation of MB dye (12 ppm) has been evaluated using one weight percent ZnS/A-FA (1 wt%) catalyst under UV light. The progress of photocatalytic dye degradation has been monitored from the UV-visible spectra at different time intervals in the presence of the ZnS/A-FA catalyst. The MB solution shows an absorption peak at 664 nm and the peak intensity decreases with increasing irradiation time (Fig. 10). It has been observed that complete degradation of MB occurs within 90 min for 1 wt% ZnS/A-FA. The colour changes that have been observed with respect to time (inset figure) indicate the progress of the dye degradation process. The complete demineralization of the MB dye suggests that the dye degradation process occurs more efficiently in the presence of the ZnS/A-FA nanocomposite, and that it will be a promising photocatalyst for the waste water treatment process. Hence, fly ash is a good supporting material for ZnS nanoparticles toward photocatalytic activities.

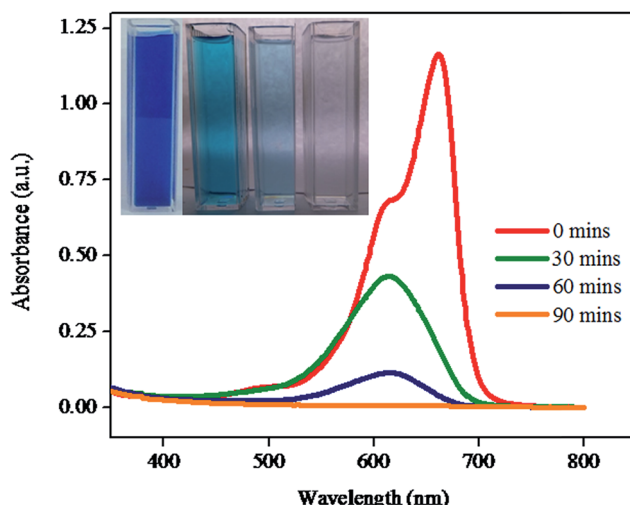


Fig. 10 Absorbance spectra showing the photodegradation of MB using ZnS/A-FA (1 wt%) nanocomposite.

Fig. 11 shows the percentage degradation of MB dye under UV irradiation in the presence of different compositions of the ZnS/A-FA nanocomposite, A-FA, and bare ZnS, and without photocatalyst. Further, dye degradation experiments are performed under dark conditions for the A-FA and ZnS/A-FA materials. In the absence of catalyst, the rate of photodegradation is found to be very low and the rate constant values almost remain constant with respect to time. The photocatalytic activity of the A-FA material and various weight percentages of ZnS/A-FA nanocomposite through sorption at different time intervals has been analyzed (Fig. 12). In the dark, the percentage of dye removed through sorption shows that only a small quantity (negligible amount) of dye has been removed due to the adsorption of the dye on the catalyst surface. From the

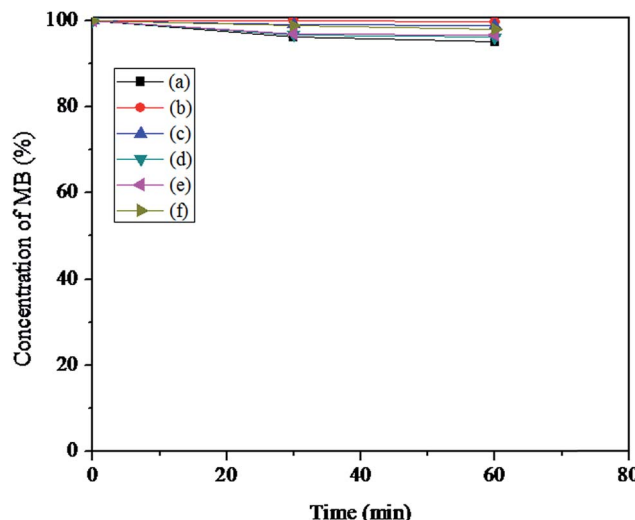


Fig. 12 Adsorption of MB dye solution in the dark for (a) A-FA, (b) 0.25 wt% ZnS/A-FA, (c) 0.5 wt% ZnS/A-FA, (d) 1 wt% ZnS/A-FA, (e) 2 wt% ZnS/A-FA and (f) 3 wt% ZnS/A-FA nanocatalyst.

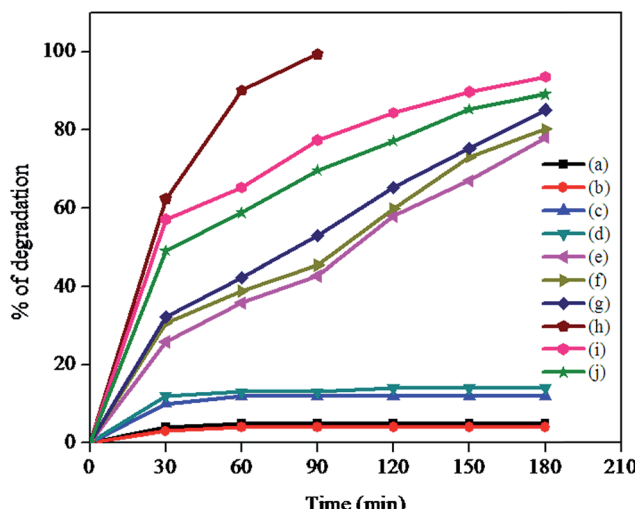


Fig. 11 Photodecomposition of MB dye solution: (a) A-FA (dark), (b) ZnS/A-FA (dark), (c) without catalyst, (d) A-FA, (e) bare ZnS, (f) 0.25 wt% ZnS/A-FA, (g) 0.5 wt% ZnS/A-FA, (h) 1 wt% ZnS/A-FA, (i) 2 wt% ZnS/A-FA and (j) 3 wt% ZnS/A-FA nanocomposite under UV irradiation.

results, it has been concluded that the adsorption process remains constant after 30 min under dark conditions. Further, it has been noticed that there is no significant colour change taking place in the dye solution. These observations show that UV light and photocatalyst are essential for the degradation of MB dye. Hence, it has been proved that dye removal takes place due to the catalytic photochemical reaction. So, the photocatalysts, namely bare ZnS, 0.25 wt% ZnS/A-FA, 0.5 wt% ZnS/A-FA, 1 wt% ZnS/A-FA, 2% ZnS/A-FA and 3 wt% ZnS/A-FA, are evaluated under similar experimental conditions and their corresponding percentages of degradation are reported (curve e-j). From the above results, it has been observed that the photocatalytic activity of the ZnS/A-FA (1 wt%) nanocomposite increased more efficiently compared to ZnS nanoparticles.⁴⁶ Further, compared with the other ratios, the one weight percent ZnS/A-FA photocatalyst degrades the MB dye more effectively and achieves complete photodegradation of the MB dye within 90 min under UV irradiation. Hence, the above studies confirm that the one weight percent ZnS/A-FA nanocomposite can work as an efficient catalyst for dye degradation for textile and waste water treatment applications.

Kinetics studies

The photocatalytic degradation of MB dye in the presence of ZnS/A-FA follows pseudo first order kinetics. When the initial dye concentration is low, the rate expression is given by

$$\frac{dC}{dt} = k'[C] \quad (2)$$

where k' is the pseudo-first order rate constant. The integrated form of the eqn (2) is given as follows:

$$\ln \frac{C_0}{C} = kt \quad (3)$$

where C_0 – concentration of dye at equilibrium, C – concentration at time ' t ' and k – rate constant.

The photocatalyst and the dye solution are initially stirred for about 30 min so that the dye in the solution gets adsorbed on the surface of the ZnS/A-FA composite. Thus, the adsorption–desorption equilibrium is achieved between the dye and the photocatalyst. After the adsorption process, the equilibrium concentration of the dye solution is determined and is taken as the initial dye concentration for kinetic analysis. The photocatalytic performance of dye degradation is affected by pH, catalyst dosage and concentration of dye. Hence, the kinetic studies were carried out by varying the pH, catalyst dosage and concentration of dye.

Effect of pH

The pH of the solution determines the surface properties of the catalyst, charge of the dye molecules, dye adsorption ability on the surface of the catalyst and the availability of hydroxyl radicals in the nanocomposite.⁴⁷ So, the pH also greatly influences the rate of photodegradation of the dye molecules under UV irradiation. The pH of the aqueous solution is adjusted before irradiation by addition of either HCl or NaOH solution. Fig. 13 displays the degradation of MB dye at various pH values in the range of 3 to 13. From Fig. 13, it has been concluded that the dye degradation follows pseudo first order kinetics. Further, it has been observed that the degradation efficiency of the MB dye increases when moving from pH 3 to 9. However, a further increase in the pH value is attributed to a decrease in the rate of photodegradation. Normally, at acidic pH, the surface of the photocatalyst becomes positively charged. Therefore, at low pH the H^+ ions compete effectively with the dye molecules so the removal efficiency of the catalyst is found to be less. At higher pH, the availability of hydroxyl ions will be greater, and they will react with holes to form hydroxyl radicals. Hence, the photocatalytic activity increases with increasing pH. However, the decolorization of the dye molecules is reduced when the pH is above 11, which is due to competing adsorption of hydroxyl ions over the dye molecules on the catalyst surface.⁴⁸

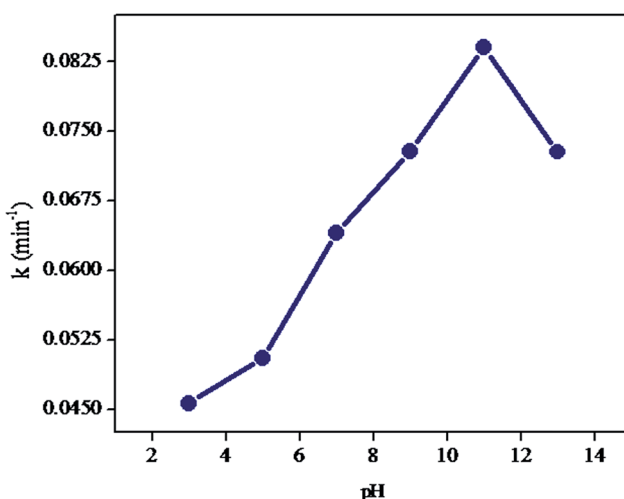


Fig. 13 Plot of pH vs. rate constant of photodegradation of MB dye solution (12 ppm) in the presence of ZnS/A-FA (1 wt%) nanocomposite with an irradiation time of 30 min.

Effect of catalyst loading

The photodegradation of 12 ppm MB dye solution has been carried out under UV irradiation with varying catalyst dosages of 30, 50, 70, 100 and 120 mg, after achieving adsorption–desorption equilibrium between the dye and catalyst. Fig. 14 shows the rate of photodegradation of the dye at different dosages of catalyst after 30 min UV irradiation. Under these experimental conditions, the degradation of MB dye on ZnS/A-FA exhibits a pseudo first order reaction. The rate of dye degradation increases with an increase in the catalyst dosage from 10 to 120 mg. The degradation efficiency of MB dye has been found to be optimized and there is no further significant increase in the rate of photodegradation, which is due to the light scattering effect of the catalyst.

Effect of dye concentration

The effect of MB dye concentration on the ZnS/A-FA composite is determined by using 4, 6, 8, 10, 12 and 14 ppm of MB dye solution after 30 min UV irradiation. Fig. 15 shows the effect of dye concentration on the ZnS/A-FA (1 wt%) nanocomposite under UV irradiation after 30 min. On increasing dye concentration from 6–12 ppm, the number of dye molecules adsorbed on the catalyst surface is also increased. So, the expected result is to enhance the photocatalytic activity. However, at the initial stage (irradiation time: 30 min) as the dye concentration increases, the penetration of photons towards the catalyst surface, which generates the hydroxyl radicals for the dye degradation process, is reduced.⁴⁹ So, the rate of photodegradation of the dye decreases as the concentration of dye increases.

Mechanism of photodegradation of MB over the ZnS/A-FA nanocomposite

A possible mechanism of dye degradation on the ZnS/A-FA nanocomposite has been hypothesized based on the studies

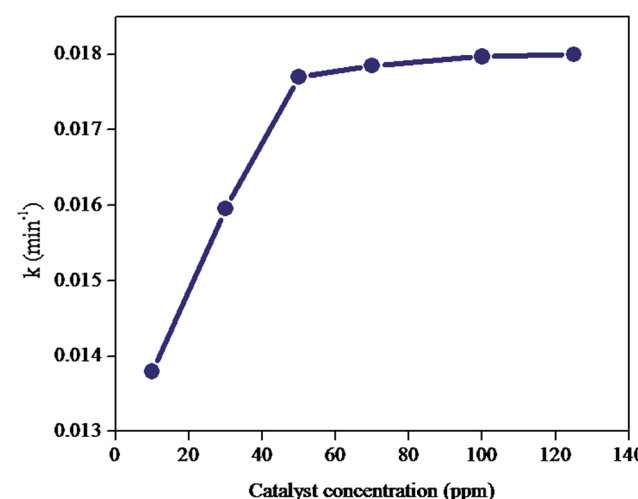


Fig. 14 Plot of catalyst concentration vs. rate constant of photodegradation of 12 ppm MB dye solution on ZnS/A-FA (1 wt%) nanocomposite with an irradiation time of 30 min.

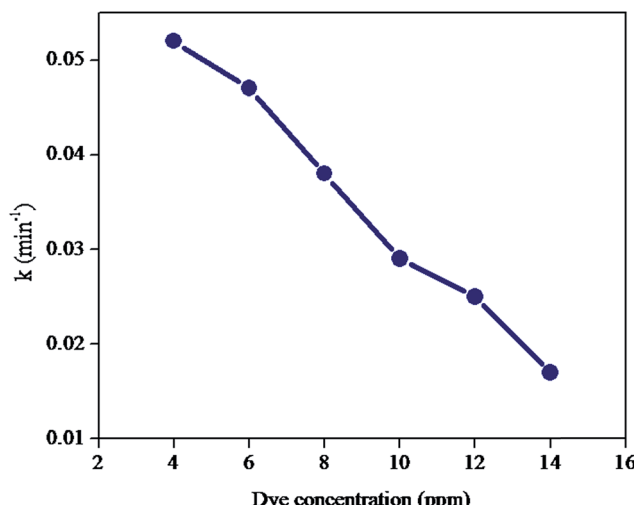


Fig. 15 Plot of dye concentration vs. rate constant of MB dye solution degradation with ZnS/A-FA (1 wt%) nanocomposite with irradiation time of 30 min.

of the important factors that affect the rate of reaction (Scheme 1).

Upon UV irradiation, the electrons are excited in the valence band (VB) of ZnS and are ejected into the conduction band (CB), thereby creating holes (h^+) in the VB. The photogenerated electrons react with oxygen (O_2) to generate super oxide anion radicals ($\cdot O_2^-$) and holes that react with water (H_2O) to produce the hydroxyl radicals (OH^-). The formation of the above radicals leads to degradation of the adsorbed MB dye over the ZnS/A-FA nanocomposite. Further, the presence of semiconductors over the supporting material inhibits the recombination of electron-hole pairs. Hence, the ZnS/A-FA composite shows enhanced photocatalytic dye degradation when compared to bare ZnS nanoparticles.

To provide evidence for the photocatalytic mechanism, isopropanol has been chosen for the detection and quantification of OH radicals. Isopropanol can be easily oxidized by OH⁻ radicals. Hence, the isopropanol can quench the OH⁻ radicals

and photocatalytic activity is reduced. The effects of isopropanol concentration (0.1 M and 1 M) are determined for the photodegradation of MB dye (Table 1) and the results show that a decrease in degradation efficiency has been observed with an increase in the concentration of isopropanol. This is due to the chemical reaction between isopropanol (hydroxyl radical scavenger) and OH⁻ radicals that quenches the photocatalytic reaction.⁵⁰ Thus, the present investigation concludes that OH⁻ radicals are generated during the dye degradation experiments, which could support the dye degradation mechanism.

Antimicrobial properties

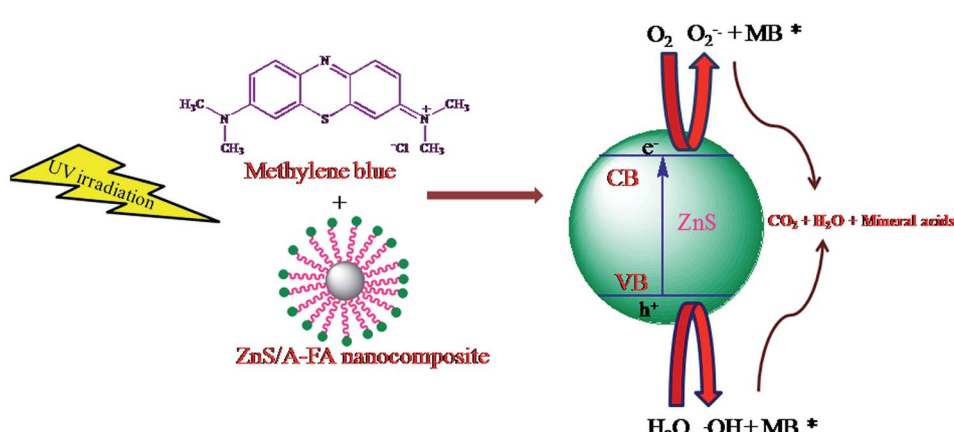
The antimicrobial properties of A-FA, bare ZnS nanoparticles and the ZnS/A-FA nanocomposite have been investigated against *Staphylococcus aureus* (*S. aureus*) and *Escherichia coli* (*E. coli*) microorganisms. The effect of addition of various concentrations of A-FA, ZnS and ZnS/A-FA nanocomposite to the microorganisms are presented in the Fig. 16 and 17.

The diameter of the zones around the discs illustrates the inhibition of bacterial growth. The A-FA material (Fig. 16) exhibits no significant changes in antibacterial activity against *S. aureus* and *E. coli*. Surprisingly, from the results it has been observed that the antibacterial properties of the ZnS/A-FA nanocomposite are enhanced considerably compared to bare ZnS particles (Fig. 17 and 18).

The improved antibacterial activity is stimulated by the interaction between the ZnS and A-FA material in the nanocomposite. The enhancement in the antibacterial activity might be attributed to the small size of the ZnS on the A-FA, large

Table 1 Effect of isopropanol on the photodegradation efficiency of the MB dye (60 min)

Quencher	Degradation (%)
No quencher	90.11
0.1 M isopropanol	80.25
1 M isopropanol	63.06



Scheme 1 Proposed mechanism for the photodegradation of MB dye on ZnS/A-FA nanocomposite under UV irradiation.

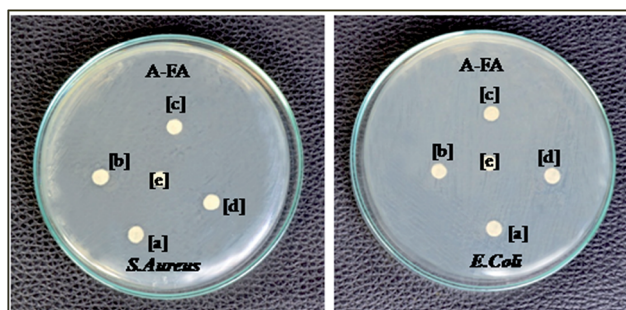


Fig. 16 Images of Petri dishes showing the antibacterial properties of A-FA material of different concentrations (a–d) and the control (e).

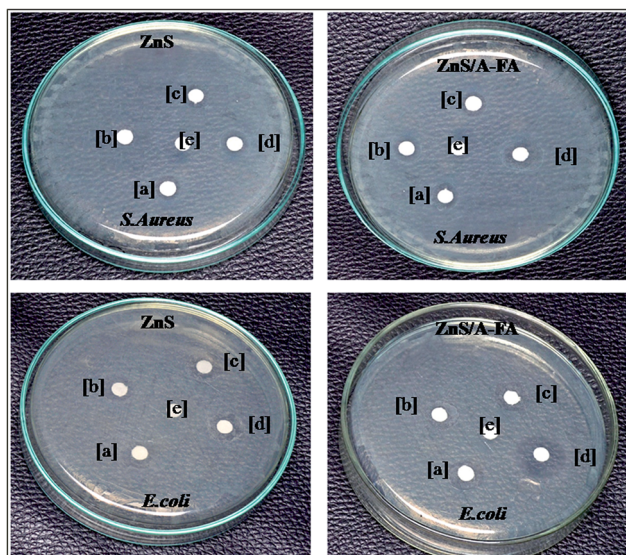


Fig. 17 Optical images of Petri dishes showing the antibacterial properties of ZnS and ZnS/A-FA nanocomposites of different concentrations (a–d) and the control (e).

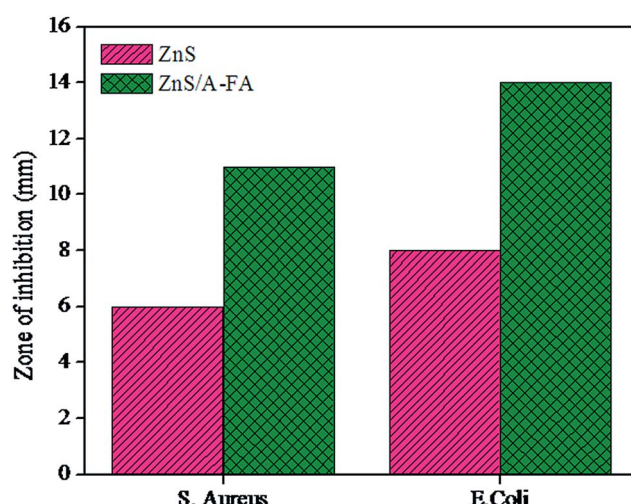


Fig. 18 Bar diagram showing antibacterial properties of ZnS and ZnS/A-FA nanocomposite against *S. aureus* and *E. coli*.

Table 2 The *t*-test statistics of antimicrobial activities of ZnS/A-FA nanocomposite compared with ZnS material against *S. aureus* and *E. coli* microorganisms

Type of the test	<i>S. aureus</i>	<i>E. coli</i>
<i>t</i> -value	14.8544	19.6463

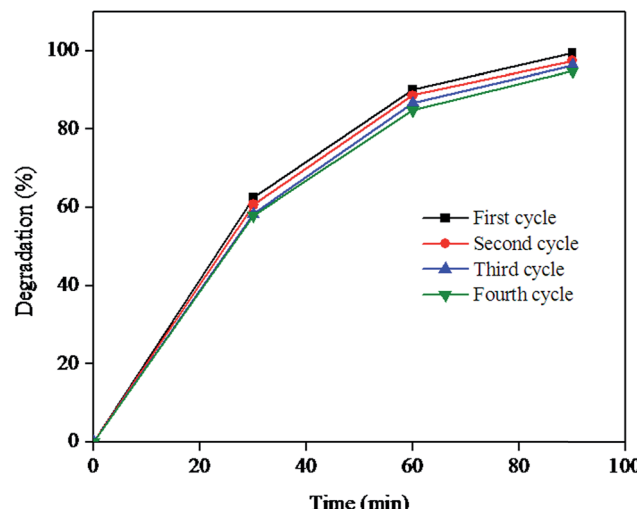


Fig. 19 Cyclic stability of ZnS/A-FA for the photocatalytic degradation of MB under UV irradiation.

specific surface area, high penetrating power and ability to effectively penetrate the outer cell membrane. The microorganism will take up the ZnS/A-FA nanocomposite due to its small size and the antimicrobial activities are considerable for a low concentration of nanocomposite. Even though ZnS has antimicrobial activity on the bacterial colonies, the nanocomposite has very high antibacterial activity, *i.e.* almost double the size of the zone of inhibition has been achieved. The bacterial activities can also occur due to the van der Waals forces between the ZnS/A-FA nanocomposite and the bacterial surface.⁵¹ However, ZnS particles are smaller in size which makes it easier for them to penetrate into the cell wall of the microorganism. As a result, the enhancement in bacterial inhibition occurs due to the cell death that takes place through cell wall decomposition. Further, the penetration of ZnS/A-FA disturbs the cell permeability, thereby leading to the leakage of minerals, proteins, and genetic material, ultimately causing cell death.⁵²

Further, the antimicrobial activities of the ZnS/A-FA material along with the ZnS material were statistically analyzed by applying *t*-tests.⁵³ The results showed that the antimicrobial activity of the ZnS/A-FA material was more significant at $P < 0.05\%$ than that of the ZnS material (Table 2).

Stability of the catalyst

The stability of the ZnS/A-FA nanocomposite has been tested to assess the reusability over four different cycles and the relative

change in the degradation percentage of MB dye is shown in Fig. 19. From the results, it has been observed that the photocatalytic reactivity of ZnS/A-FA remains effective and no significant change in the photocatalytic activity of the catalyst is noticed. Hence, the results indicated that the reuse of the ZnS/A-FA nanocomposite is feasible and its stability is found to be satisfactory.

Conclusion

In the present work, a novel ZnS/A-FA nanocomposite has been synthesized by loading ZnS on the surface of various weight% of A-FA material. The surface area of the ZnS/A-FA photocatalyst is improved by using fly ash as a supporting material, compared to that of bare ZnS nanoparticles. Further, the band gap energy of ZnS/A-FA has been reduced compared with bare ZnS nanoparticles. The TEM images reveal that the ZnS particles are finely deposited on the surface of the A-FA material through a wet chemical method. Further, the ZnS/A-FA material shows higher photocatalytic activity and antimicrobial activity compared to bare ZnS nanoparticles. So, the ZnS/A-FA nanocomposite will be a promising photocatalyst and antimicrobial agent for multipurpose industrial applications.

Acknowledgements

The authors would like to thank DST/Nanomission, New Delhi, India for financial support to carry out this work and the establishment of the Nanotech Research Lab through grant no. SR/NM/NS-05/2011(G).

References

- 1 A. X. Zeng, W. H. Xiong and J. Xu, *Surf. Coat. Technol.*, 2005, **197**, 142.
- 2 M. Vautier, C. Guillard and J. M. Herrmann, *J. Catal.*, 2001, **201**, 46.
- 3 T. Sano, N. Negishi, K. Uchino, J. Tanaka, S. Matsuzawa and K. Takeuchi, *J. Photochem. Photobiol., A*, 2003, **160**, 93.
- 4 F. Harrelkas, A. Paulo, M. M. Alves, L. E. Khadir, O. Zahraa, M. N. Pons and F. P. van der Zee, *Chemosphere*, 2008, **72**, 1816.
- 5 G. H. Tian, H. G. Fu, L. Q. Jing and C. G. Tian, *J. Hazard. Mater.*, 2009, **161**, 1122.
- 6 R. Asahi, T. Morikawa, T. Ohwaki, K. Aoki and Y. Taga, *Science*, 2009, **293**, 269.
- 7 Y. V. Kolen'ko, B. R. Churagulov, M. Kunst, L. Mazerolles and C. Colbeau-Justin, *Appl. Catal., B*, 2004, **54**, 51.
- 8 K. Chiang, T. M. Lim, L. Tsen and C. C. Lee, *Appl. Catal., A*, 2004, **261**, 225.
- 9 S. Yanagida, K. Mizumoto and C. J. Pac, *J. Am. Chem. Soc.*, 1986, **108**, 647.
- 10 J. S. Hu, L. L. Ren, Y. G. Guo, H. P. Liang, M. A. Cao, L. J. Wan and C. L. Bai, *Angew. Chem., Int. Ed.*, 2005, **44**, 1269.
- 11 S. L. Xiong, B. J. Xi, C. M. Wang, D. C. Xu, X. M. Feng, Z. C. Zhu and Y. T. Qian, *Adv. Funct. Mater.*, 2007, **17**, 2728.
- 12 X. Fang, T. Zhai, U. K. Gautam, L. Li, L. Wu, Y. Bando and D. Golberg, *Prog. Mater. Sci.*, 2011, **56**, 175.
- 13 J. M. L. Nieto, *Top. Catal.*, 2001, **15**, 189.
- 14 Y. Yu, *Powder Technol.*, 2004, **146**, 154.
- 15 M. Visa, R. A. Carcel, L. Andronic and A. Duta, *Catal. Today*, 2009, **144**, 137.
- 16 J. Shi, S. Chen, S. Wang, P. Wu and G. Xu, *J. Mol. Catal. A: Chem.*, 2009, **303**, 141.
- 17 P. Huo, Y. Yan, S. Li, H. Li and W. Huang, *Appl. Surf. Sci.*, 2009, **255**, 6914.
- 18 C. Yang, T. Wang, P. Liu, H. Shi and D. Xue, *Curr. Opin. Solid State Mater. Sci.*, 2009, **13**, 112.
- 19 J. Shi, S. Chen, S. Wang, Z. Ye, P. Wu and G. Xu, *J. Mol. Catal. A: Chem.*, 2009, **303**, 141.
- 20 P. Huo, Y. Yan, S. Li, H. Li, W. Huang, S. Chen and X. Zhang, *Desalination*, 2010, **263**, 258.
- 21 P. Huo, Y. Yan, S. Li, H. Li and W. Huang, *Desalination*, 2010, **256**, 196.
- 22 J. Shi, S. Chen, S. Wang, Z. Ye, S. Wang and P. Wu, *Appl. Surf. Sci.*, 2010, **257**, 1068.
- 23 J. Shi, S. Chen, S. Wang, Z. Ye, P. Wu and B. Xu, *J. Mol. Catal. A: Chem.*, 2010, **330**, 41.
- 24 P. Huo, Y. Yan, S. Li, H. Li and W. Huang, *Appl. Surf. Sci.*, 2010, **256**, 3380.
- 25 Z. Shi, S. Yao and C. Sui, *Catal. Sci. Technol.*, 2011, **1**, 817.
- 26 B. Wang, Q. Li, W. Wang, Y. Li and J. Zhai, *Appl. Surf. Sci.*, 2011, **257**, 3473.
- 27 Z. Shi, S. Yao and C. Sui, *Catal. Sci. Technol.*, 2011, **1**, 817.
- 28 B. Wang, C. Li, J. Pang, X. Qing, J. Zhai and Q. Li, *Appl. Surf. Sci.*, 2012, **258**, 9989.
- 29 J. Zhang, H. Cui, B. Wang, C. Li, J. Zhai and Q. Li, *Chem. Eng. J.*, 2013, **223**, 737.
- 30 A. N. Okte and D. Karamanis, *Appl. Catal., B*, 2013, **142**, 538.
- 31 M. Kuppayee, G. K. V. Nachiyar and V. Ramasamy, *Appl. Surf. Sci.*, 2011, **257**, 6779.
- 32 M. Antoniadou, V. M. Daskalaki, N. Balis, D. I. Kondarides, C. Kordulis and P. Lianos, *Appl. Catal., B*, 2011, **107**, 188.
- 33 M. El-Kemary and H. El-Shamy, *J. Photochem. Photobiol., A*, 2009, **205**, 151.
- 34 V. Stengl, V. Houskova, S. Bakardjieva and N. Murafa, *ACS Appl. Mater. Interfaces*, 2010, **2**, 575.
- 35 K. M. Reddy, S. V. Manorama and A. R. Reddy, *Mater. Chem. Phys.*, 2002, **78**, 239.
- 36 A. Goudarzi, G. M. Aval, S. S. Park, M. C. Choi, R. Sahraei, M. H. Ullah, A. Avane and C. S. Ha, *Chem. Mater.*, 2009, **21**, 2375.
- 37 S. Biswas, S. Kar and S. Chaudhari, *J. Phys. Chem. B*, 2005, **109**, 17526.
- 38 R. C. Pawar and C. S. Lee, *Appl. Catal., B*, 2014, **144**, 57.
- 39 N. A. Dhas, A. Zaban and A. Gedanken, *Chem. Mater.*, 1999, **11**, 806.
- 40 X. Zhang, Y. Tang, Y. Li, Y. Wang, X. Liu, C. Liu and S. Luo, *Appl. Catal., A*, 2013, **457**, 78.
- 41 P. Huo, Y. Yan, S. Li, H. Li and W. Huang, *Appl. Surf. Sci.*, 2010, **256**, 3380.
- 42 J. C. Yu, L. Z. Zhang and J. G. Yu, *Chem. Mater.*, 2002, **14**, 4647.

- 43 L. Wu, J. C. Yu, X. C. Wang, L. Z. Zhang and J. G. Yu, *J. Solid State Chem.*, 2005, **178**, 321.
- 44 L. H. Zhang, H. Q. Yang, J. Yu, F. H. Shao, L. Li, F. H. Zhang and H. Zhao, *J. Phys. Chem. C*, 2009, **113**, 5434.
- 45 J. G. Yu, J. C. Yu, M. K. P. Leung, W. Ho, B. Cheng, X. Zhao and J. Zhao, *J. Catal.*, 2003, **217**, 69.
- 46 S. K. Apte, S. N. Garaje, S. S. Arbuji, B. B. Kale, J. O. Baeg, U. P. Mulik, S. D. Naik, D. P. Amalnerkara and S. W. Gosavi, *J. Mater. Chem.*, 2011, **21**, 19241.
- 47 B. Subash, B. Krishnakumar, B. Sreedhar, M. Swaminathan and M. Shanthi, *Superlattices Microstruct.*, 2013, **54**, 155.
- 48 M. Shamsipur and H. R. Rajabi, *Spectrochim. Acta, Part A*, 2014, **122**, 260.
- 49 B. Krishnakumar, K. Selvam, R. Velmurugan and M. Swaminathan, *Desalin. Water Treat.*, 2010, **24**, 132.
- 50 Y. Chen, S. Yang, K. Wang and L. Lou, *J. Photochem. Photobiol. A*, 2005, **172**, 47.
- 51 J. vandiver, D. Dean, N. Patel, C. Botelho, S. Best, J. D. Santos, M. A. lopes, W. Bondield and C. Ortiz, *J. Biomed. Mater. Res., Part A*, 2006, **78**, 1619.
- 52 P. K. Stoimenov, R. L. Klinger, G. L. Marchi and K. J. Klabunde, *Langmuir*, 2002, **18**, 6679.
- 53 J. S. Duhan, P. Saharan and Surekha, *Asian J. Pharm. Clin. Res.*, 2013, **6**, 291.